

Appendix A: The good, the bad and the ugly of RbLi

This appendix summarizes the best, the worst and the meh aspects of the RbLi apparatus. Hopefully the items presented here are helpful to future students building experimental apparatuses for ultracold atoms.

A.1 The good

It is very easy to come up with a list of bad things that don't work quite well in the lab. Coming up with a list of good things that work well is harder; if we are not fixing a broken thing we don't think much about it. When the current postdoc was prompted with the question of what she loved most about our apparatus she answered 'I love every single thing about RbLi.' Unfortunately there is not enough space to talk about every single thing and the list below summarizes some good things in our lab.

Overkill transistor banks: Large currents in the lab (quadrupole and Zeeman slower) are controlled with MOSFET banks formed by a group of MOSFETS whose drain and source are connected in parallel and sharing the same gate voltage that is controlled by a PI servo. The Zeeman slower always operates at a fixed current but the current in the quadrupole coils is dynamically changed throughout

the experimental sequence and a fast response is desirable. In 2013 we replaced the quadrupole MOSFET bank with a new unit that contains 20 IXFN 520N075T2 transistors rated for 75 V and 480 A (left panel of Figure 1). Even though our currents never exceed 70 A, the performance of the transistors really decays as the drain to source voltage is increased as can be seen in the right panel of Figure 1. The use of more transistors reduces the power dissipation of each individual transistor which allows us to operate the power supply at a higher voltage of 15 V that helps counteract the inductive kickback of the coils. With the new transistor bank the turn on time of the coils was reduced from 100 ms to 50 ms leading to improved magnetic trapping and better Stern-Gerlach pulses for imaging, only with an unavoidable small number of blown off transistors.

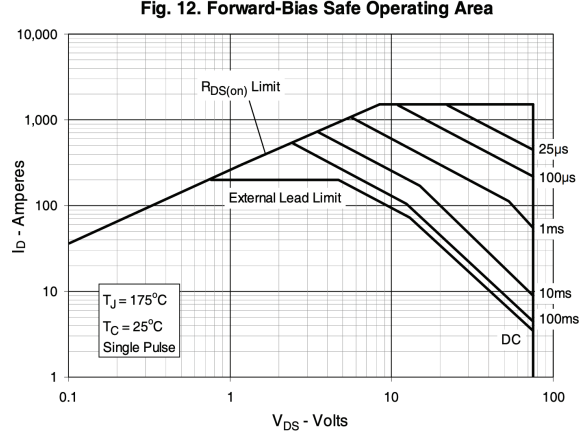
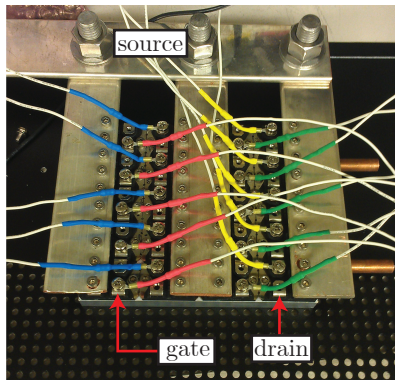


Figure 1: Left: New MOSFET bank. Right: Safe operation regime of the IXFN 520N075T2 MOSFET. Even though they are in principle rated for up to 480 A the maximum safe current is greatly reduced at larger drain to source voltages V_{DS} . A high V_{DS} is desirable to reduce the inductive kickback during turn on.

Hand made in vacuum shutters: Before going into the Zeeman slower, the atoms that were heated in the Rb oven travel to the main oven chamber that is

pictured in Figure 2b containing a cold-cup and an oven shutter. The cold-cup is a cylindrical shaped copper piece that is attached to the cold end of a thermo-electric cooler (TEC) via a copper rod. We keep the cold-cup temperature at -30 C in order to capture excess Rb atoms in the chamber and prevent damaging the ion pumps. The oven shutter allows us to block after the MOT loading stage to prevent unwanted heating. We use a homemade device, made from a re-purposed hard drive disk shutter with a metallic flag attached to its end. The shutter is electrically connected to an electric feedthrough with vacuum-compatible Kapton sealed wires. Other apparatus within the JQI [1] have commercial shutters from Uniblitz and some of them have failed in the past. Overall we have found this setup to be very reliable. The only problem we experienced once was some accumulation of Rb on the cold cup that started blocking the atomic beam. To remedy this we reversed the polarity of the TEC and heated the cold cup barely enough so that the accumulated Rb atoms melted and moved away from the aperture of the atomic beam.

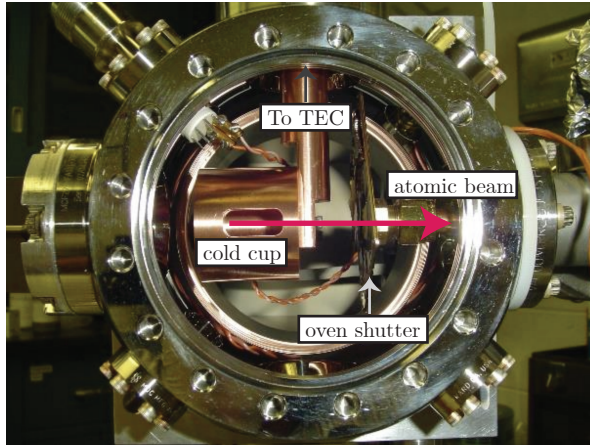


Figure 2: The RbLi oven chamber. We use a homemade in-vacuum shutter to block the atomic beam after the MOT stage to prevent heating of the atoms at later stages.

Ultraviolet LEDs: We have two 3 W ultraviolet LEDs from **Mightex** placed at the glass cell side of the vacuum system. One is aimed at the vacuum window where the slower beam enters and the other is placed aiming at the glass cell. The LEDs prevent Rubidium from depositing on the vacuum system and can conveniently be turned on and off with a TTL signal from the computer. We have found that routinely turning them on (for example, leaving them on overnight) leads to a smoother operation of the system.

Mirror mounts with picomotor actuators: We use 8816-6 picomotor optical mounts from **New Focus Optics** whose deflection angle can be electronically adjusted on the order of microradians. The addition of picomotor mounts has made alignment of laser beams to the atoms significantly easier. We use this mounts on the last tunable mirror before the atoms for beam paths whose alignment is critical, for example in optical dipole trap and Raman beams.

Polarizers on MOT beams: The light of our MOT beams is coupled to polarization maintaining optical fibers. We found that besides our best efforts to align the polarization of the incoming light to the axis of the fiber the fluctuations in the output polarization could cause considerable instabilities in the BEC production. To keep the polarization clean we placed polarizers at the output of the fibers. We found that despite the power hit we can get from the changes in polarization, this solution leads to a much more stable production of BECs.

Lab couch: When the experiment is functional enough that data can be taken long hours in the lab are often required. If it gets late, the lab couch allows the person running the experiment to take small naps as the data keeps coming while

still being close to the apparatus in case something needs to be fixed.

Other elements already mentioned in the main text: The new master laser from Vescent photonics has been very stable and reliable. The new Mako camera has been very helpful to get rid of unwanted fringes in absorption images. Labscript makes writing experimental sequences very straightforward.

A.2 The bad

The bad, these are elements of the apparatus that were constant sources of pain and if considering a new experimental design should be avoided.

Water cooling shared between two labs: The quadrupole and Zeeman slower coils as well as the transistor banks require water cooling due to Joule heating. Our lab space is shared with a Rubidium-Ytterbium ultracold mixtures apparatus [2] and amongst the things we shared is the water cooling system. The schematic in Figure 3 illustrates the layout of the water cooling system. The water was filtered at two different points, first at each line has a $440\ \mu\text{m}$ particulate filter from Swagelok and then the water returning to the heat exchanger is filtered with a low-impedance cellulose cartridge (McMaster 7191K11). Both filters only capture impurities in the water for one given flow direction. One of the failure modes which occurs when one of the booster pumps is turned on before the heat exchanger, causing water to flow from one experiment to the other and bringing a collection of nasty things that escapes the filters into the coils. Over the years our system has suffered of clogged filters, clogged coils and broken booster pumps. For best operation it is

highly recommended that the cartridge filter is changed and that the Swagelok filters be cleaned at least once a year and that a 10% solution of an anti-corrosive Optishield Plus in water is used as a coolant. Even when following this practices, we managed to find lots of gunk and unidentified objects (sand? glass? mud? oxide? dead bacteria?) in the water, just at a slower rate.

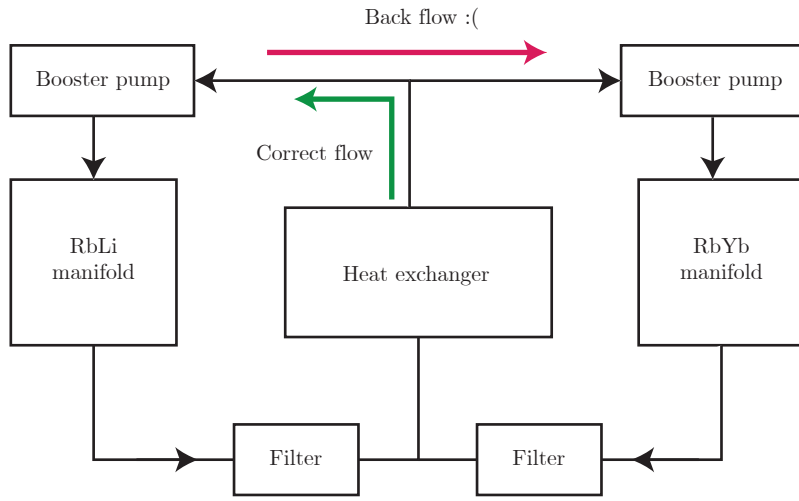


Figure 3: Simplified schematic of the shared water cooling manifold.

Flipper mirrors: The optical path of the MOT beams near the atoms is very close to that of Raman, optical dipole trap and probe beams. Since the MOT beams are only used at the early stages of the experiment it is tempting to use flipper mirror mounts so that once they are no longer needed they can be moved away to make space for other beams. This was the approach originally taken in the lab and we used 8893-K motorized optical flipper mounts from Newport in multiple locations. As they break over and over again, they have been slowly replaced by more stable solutions such as periscopes or polarizing beam splitters wherever it is

possible. Flipper mirrors are always bound to break, it is only a matter of time.

Avoid using them unless you absolutely have no alternative.

Optical fibers right below air vents: The optical fibers connecting the main experiment optical table and the laser optical table are routed close to a pair of AC vents in the lab. The changes in air temperature result in polarization fluctuations at the output of optical fibers, a constant cause of pain and instability in our BEC production. We have tried to remedy this issue by partially blocking vents and enclosing the fibers in a large PVC tube.

Free space dipole laser: The laser system providing 1064 nm light for the optical dipole trap is not fiber coupled and is setup in the same optical table as the vacuum system; we are not able to change the laser without destroying the alignment of the beam with the atoms. This issue became important while setting up a 1D optical lattice by retro-reflecting one of the dipole trap beams we noticed that the laser mode is not very stable, leading to big fluctuations in the optical lattice. In the original design of the laser system high-power photonic crystal fibers were included but they did not have built in mode expanders which resulted in the tip of the fiber inevitably getting burnt after some time of use. In short, mode expanders are recommended in applications involving large optical powers.

A.3 The ugly

The ugly elements are not quite bad but they don't function flawlessly either. If given the option to replace them with something better I definitely would.

Kepco bipolar power supplies: We use three Kepco BOP 20-20M bipolar power supplies to provide the current for the bias coils. While it is nice to have a commercially available power supply that can provide $\pm 20\text{ A}$ they come with a few drawbacks. First the current they provide has 60 Hz noise in it and in order to suppress it and stabilize the currents we must use a PI feedback circuit. The power supplies has multiple banks of NPN and PNP transistors inside mounted on a big heat sink with fans attached to it making them quite noisy; it is not optimal to place them close to the main experiment chamber and long connections open the door to unwanted ground loops. Additionally they have a few failure modes. The most common problem we experienced was output current would rail, which is related to broken transistors which tend to inevitably fail after some time. Many of the symptoms of broken Kepcos spoken by other labs seem to usually boil down to malfunctioning transistors.

Toptica's BoosTA: Our cooling light comes from a Toptica DL Pro is amplified using a Toptica BoosTA tapered amplifier system. While the output power of this TA has been relatively stable over the years it has a tendency to turn itself off. On its bad days it would turn off so often that it would be impossible to operate the experiment. We haven't been able to identify the problem despite our best efforts to look into the TA controller, the TA itself, multiple conversations with Toptica engineers etc.

Too many devices connected to the same computer: We use multiple USB-6229 data acquisition (DAQ) devices from National Instruments. They are located at different points of the lab and then connected to the control computer

through USB to optical fiber adapters that break the ground between the computer and the rest of the lab equipment (a practice we always try to follow when connecting things to the computer). We have a total of 6 NI devices in addition to other equipment like oscilloscopes all connected to the computer through BNC cables. Often times we struggled with the computer failing to detect one or multiple devices and it would take a very special (and different every time) combination of plugging and unplugging, turning off and turning back on things until all devices were recognized by the computer. We observe that the problem occurs less often when we don't have as many USB devices connected to the computer.

Appendix B: New apparatus

As mentioned in the main text, the construction of a new apparatus for producing BECs of ^{87}Rb and ^{39}K is underway. The design of the apparatus is intended to be a bug fix version of the RbChip [3] lab at NIST. The new apparatus does not have a Zeeman slower and instead will use magnetic transport coils to move atoms from a MOT cell to the main science cell.

This Appendix describes some aspects of the design and construction of the new apparatus where I was involved. Disclaimer: none of this things have been tested yet so we don't know yet if it will all work horribly. I have listed all relevant part numbers in case replacements are needed.

B.1 Water cooling

The lack of a Zeeman slower in the apparatus greatly simplifies the water cooling system compared to that of RbLi. Since we don't anticipate to have any coils with high flow impedance we expect that the pressure from a recirculating chiller will be enough to provide water cooling to the transistor banks and the magnetic transport coils.

Our choice of chiller was the TF1LN400-LN 1.4 kW recirculating chiller from

Thermo Fisher Scientific. The water is filtered both at the output and the return with a high-impedance filter with a cellulose cartridge (filter: McMaster 4422K3, cartridge: McMaster 7191K11). A breakout manifold divides the chilled water into 5 different lines, each one with a flow meter (Proteus Industries 0101C110) that can be used to interlock the current of water cooled applications to the flow of water. Based on previous experiences with plumbing (see Appendix A) I highly encourage replacing the filters at least once a year and to use a solution of 10% corrosion inhibitor (e.g. OptiShield Plus) and distilled water as a coolant.

a. Service corridor side



b. Experiment side

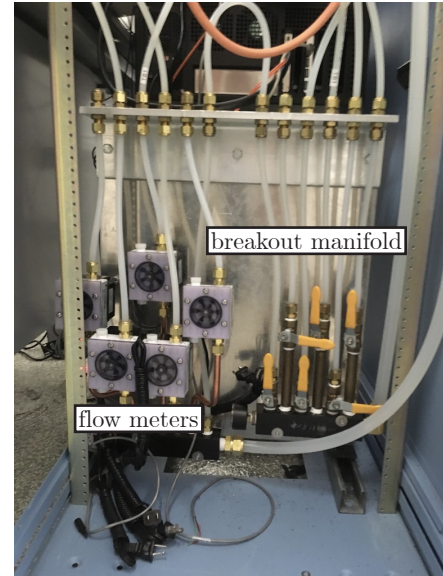


Figure 1: Water cooling

B.2 Electrical installation

We have two Agilent 6690A (440 A at 15 V max. current) to provide all the necessary currents. The power supplies are located in the service corridor and are

connected to three copper bars corresponding to $\pm 15\text{ V}$ and ground using welding cable (McMaster 7818A17) that is laid on cable trays (McMaster 30065T11 e.g.). The cables are arranged in the pattern shown in Figure xxx so that the magnetic field produced by them is closer to a magnetic quadrupole which decays faster than the field of a magnetic dipole. We are not planning to use commercial bipolar power supplies in this lab (see Appendix A) and instead we will be using a MOSFET based homemade device that will draw current from the $\pm 15\text{ V}$ rails.

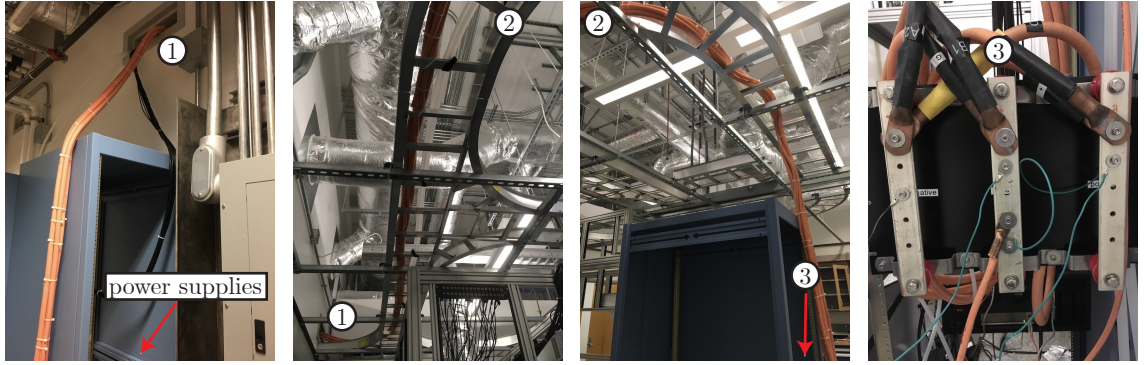


Figure 2: A roller coaster ride, from the power supplies in the service corridor to three copper bars that distribute the power.

B.3 Coil winding

All the coils in the apparatus including magnetic transport, bias and gradient cancellation have been wound using Laminax ribbon wire from Bridgeport Magnetics. We followed the coil fabrication process described in [3] which involves first winding a fixed number of turns around a prefabricated form with a particular geometry. The coils were then covered with a machinable epoxy (Stycast 1266) to fill in any air gaps. A lesson we learned while doing this is that only room

temperature epoxy should be mixed. We keep the epoxy in a fridge to extend its lifetime but if it is cold some tiny drops of water will condense in it as it is being mixed and it will not properly be cured. To minimize the air bubbles we placed the coils with epoxy on a vacuum bell and we pumped the air out using an electric vacuum pump ([McMaster 4396K21](#)). After the epoxy has cured (overnight if it is left at room temperature or less if it is left at higher temperature) the coils are ready for lathing to remove all excess epoxy and kapton tape up to the surface of the copper. After some trial and error (and lots of frustration) we found that using a diamond tip cutter ([McMaster 3316A32](#)) and spinning the lathe not faster than 150 rpm the best results. Using a cutter that is not sharp enough or cutting too aggressively close to the soft copper results in deformed rather. In the past when coils were fabricated at NIST a lathing form was used to mount the coils on the lathe. The machinist at UMD considered this was not safe enough so I instead mounted the coils using a 6 jaw chuck as shown in Figure 3a. than cut traces that merge into each other causing unwanted shorts. For anyone making coils in the future: it is sort of an art to get it right and screwing up many coils is part of learning the art.

B.4 Rb source and ‘oven’

The Rb source consists of a 1.33” CF flanged bellow ([Kurt J. Lesker MH-CF-A03](#)) with a Rb ampule . The bellow is housed in a cold ‘oven’ which is designed to keep the source at a temperature $\approx 1\text{ C}$ to keep the vapor pressure low. The oven is made of hollow aluminum cylinder with a slit on one side with tapped holes so that

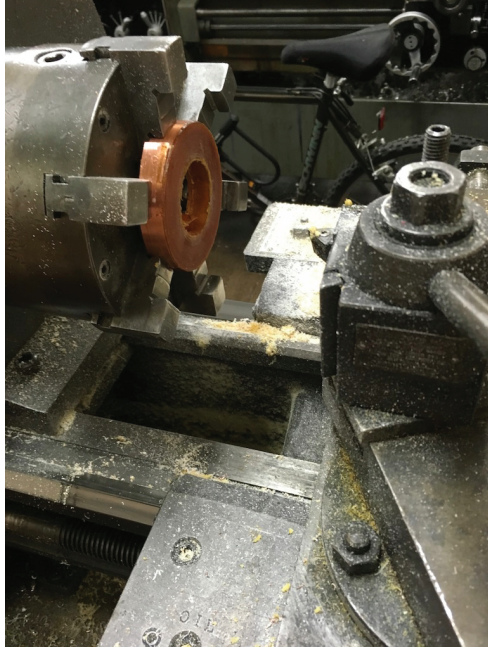


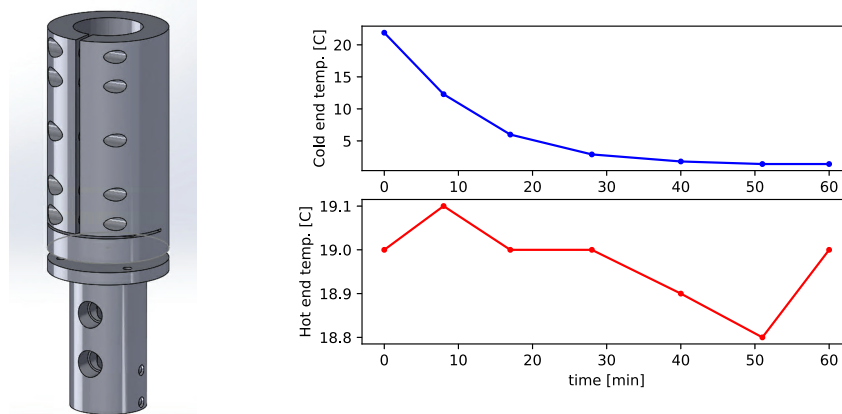
Figure 3: A roller coaster ride, from the power supplies in the service corridor to three copper bars that distribute the power.

1/4 – 20 screws can be used to fix the oven to the source. The bottom of the oven attaches to the cold end of a TEC that provides the cooling. The hot side of the TEC is attached to a heat sink made of a hollow brass piece with tapped holes for 1/4” NPT pipes are used to provide water cooling. The left panel of Figure xxx shows CAD drawings of the oven both of this parts and the right panel shows the actual parts mounted on a test bench. The Rb source will be connected to the MOT glass cell; the plan is to use light induced atomic desorption (LIAD) [4] to increase the Rb vapor pressure for MOT loading using non-thermal means.

Our initial hope was to control the temperature using a linear temperature controller designed at the JQI (the design is available at the [JQI GitHub](#)) inter-

faced to the lab computer and Labscript using a serial to ethernet adapter (WIZnet WIZ107SR). Unfortunately this project is not completed to this date.

a. Rb ‘oven’ and heat sink b. Bench test temperatures



c. Testing prototype oven and heat sink



Figure 4: Rubidium oven assembly

B.5 Table enclosures

The enclosures of the optical tables are made of **Alumalite** from **Laminators Inc.** mounted on frames made out of aluminum extrusions from 80/20 and sliding tracks (2220 and 2210). Alumalite is a sandwich of a corrugated polypropylene material in between two thin sheets of aluminum. We chose this ma-

terial because it is strong and lightweight. Its laser safety properties remain to be tested but we anticipate it is better than the acrylic panels at the RbLi lab. The initial frames were designed and built mostly by former graduate student Daniel Campbell and later finished and modified by former undergraduate student Eliot Fenton and me.

To the new and future members of the lab: I sincerely hope the things I designed and built don't cause you much pain!

Appendix C: Full derivation of the Raman coupled $|xyz\rangle$ states

In this Appendix I derive the full time-dependent Hamiltonian describing the Raman coupled $|xyz\rangle$ states. The system is based on the theoretical proposal in [5] to engineer an effective Rashba-type Hamiltonian using three Raman laser beams.

We consider an $F = 1$ system that is subject to a constant magnetic field $B_0 \mathbf{e}_z$ and an RF magnetic field $B_{RF} \cos(\omega_{RF}t) \mathbf{e}_x$. The system is described by the Hamiltonian

$$\hat{H}_{RF} = \omega_0 \hat{F}_z - \frac{\epsilon}{\hbar} (\hat{F}_z^2 - \mathbb{I}) + 2\Omega_{RF} \cos(\omega_{RF}t) \hat{F}_x, \quad (\text{C.1})$$

where $\omega_0 = g_F \mu_B B_0$ is the Larmor frequency, ϵ is a quadratic Zeeman shift that breaks the degeneracy of the $|m_F = -1\rangle \leftrightarrow |m_F = 0\rangle$ and $|m_F = 1\rangle \leftrightarrow |m_F = 0\rangle$ transitions, and $\Omega_{RF} = g_F \mu_B B_{RF}/2$ is the RF coupling strength. We then transform the Hamiltonian into a rotating frame using the unitary transformation $\hat{U}(t) =$

$\exp(-i\omega_{RF}t\hat{F}_z)$. The spin-1 operators under this transformation are transformed as

$$\begin{aligned}
 \hat{F}_x &\rightarrow \cos(\omega_{RF}t)\hat{F}_x - \sin(\omega_{RF}t)\hat{F}_y \\
 &= e^{i\omega_{RF}t}\hat{F}_+ + e^{-i\omega_{RF}t}\hat{F}_- \\
 \hat{F}_y &\rightarrow \sin(\omega_{RF}t)\hat{F}_x + \cos(\omega_{RF}t)\hat{F}_y \\
 &= \frac{1}{i}(e^{i\omega_{RF}t}\hat{F}_+ - e^{-i\omega_{RF}t}\hat{F}_-) \\
 \hat{F}_z &\rightarrow \hat{F}_z.
 \end{aligned} \tag{C.2}$$

The unitary evolution in the rotating frame is described by the transformed Hamiltonian $\hat{U}^\dagger(t)(\hat{H}_{RF} - i\hbar\partial_t)\hat{U}(t)$, which after neglecting terms that are oscillating at $2\omega_{RF}$ is

$$\hat{H}_{RWA} = \Delta\hat{F}_z - \frac{\epsilon}{\hbar}(\hat{F}_z^2 - \mathbb{I}) + \Omega_{RF}\hat{F}_x \tag{C.3}$$

The eigenstate of Equation C.3 are the $|xyz\rangle$ states described in Chapter ???. I will show later that all states can be coupled using a combination of the \hat{F}_x , \hat{F}_y , and \hat{F}_z operators in the lab frame, i.e. using different combinations of Raman laser beams with appropriately chosen polarizations.

For simplicity I will start this description in the lab frame and I will not make any initial assumptions about direction of propagation or frequency each of the beams. Consider three linearly polarized Raman beams propagating along the xy plane as shown in Fig. 1. The electric field at the atoms is

$$\mathbf{E}(x, t) = \sum_{i=1}^3 E_i \mathbf{e}_i e^{i(\mathbf{k}_i \cdot \mathbf{x} - \omega_i t)}, \quad (\text{C.4})$$

where E_i is the field amplitude, ω_i is the angular frequency, and \mathbf{e}_i is the polarization of each of the beams. In order to generate the necessary Raman couplings proportional to \hat{F}_x , \hat{F}_y and \hat{F}_z we need two horizontally polarized Raman beams and one vertically polarized beam. Without loss of generality we choose

$$\begin{aligned} \mathbf{e}_1 &= \frac{(k_{1y}, -k_{1x}, 0)}{\|\mathbf{k}_1\|^2}, \\ \mathbf{e}_2 &= (0, 0, 1), \\ \mathbf{e}_3 &= \frac{(k_{3y}, -k_{3x}, 0)}{\|\mathbf{k}_3\|^2}, \end{aligned} \quad (\text{C.5})$$

The Raman Hamiltonian is given by the vector component of the Stark shift generated by the atom-light interaction

$$\hat{H}_R = (i u_v \mathbf{E} \times \mathbf{E}^*) \cdot \hat{F}, \quad (\text{C.6})$$

where u_v is the vector polarizability. Now let's expand Eq. C.6 using the field at the atoms from Eq. C.4.

$$\begin{aligned}
\mathbf{E} \times \mathbf{E}^* &= (E_1^* \mathbf{e}_1 e^{-i(\mathbf{k}_1 \cdot \mathbf{x} - \omega_1 t)} + E_2^* \mathbf{e}_2 e^{-i(\mathbf{k}_2 \cdot \mathbf{x} - \omega_2 t)} + E_3^* \mathbf{e}_3 e^{-i(\mathbf{k}_3 \cdot \mathbf{x} - \omega_3 t)}) \times c.c \\
&= E_1^* E_2 (\mathbf{e}_1 \times \mathbf{e}_2) e^{i[(\mathbf{k}_2 - \mathbf{k}_1) \cdot \mathbf{x} - (\omega_2 - \omega_1)t]} + E_1^* E_3 (\mathbf{e}_1 \times \mathbf{e}_3) e^{i[(\mathbf{k}_3 - \mathbf{k}_1) \cdot \mathbf{x} - (\omega_3 - \omega_1)t]} \\
&\quad + E_2^* E_1 (\mathbf{e}_2 \times \mathbf{e}_1) e^{i[(\mathbf{k}_1 - \mathbf{k}_2) \cdot \mathbf{x} - (\omega_1 - \omega_2)t]} + E_2^* E_3 (\mathbf{e}_2 \times \mathbf{e}_3) e^{i[(\mathbf{k}_3 - \mathbf{k}_2) \cdot \mathbf{x} - (\omega_3 - \omega_2)t]} \\
&\quad + E_3^* E_1 (\mathbf{e}_3 \times \mathbf{e}_1) e^{i[(\mathbf{k}_1 - \mathbf{k}_3) \cdot \mathbf{x} - (\omega_1 - \omega_3)t]} + E_3^* E_2 (\mathbf{e}_3 \times \mathbf{e}_2) e^{i[(\mathbf{k}_2 - \mathbf{k}_3) \cdot \mathbf{x} - (\omega_2 - \omega_3)t]} \\
&= 2i \left[(\mathbf{e}_1 \times \mathbf{e}_2) \text{Im}\{E_1^* E_2 e^{i(\mathbf{k}_{21} \cdot \mathbf{x} - \omega_{21} t)}\} \right. \\
&\quad \left. + (\mathbf{e}_1 \times \mathbf{e}_3) \text{Im}\{E_1^* E_3 e^{i(\mathbf{k}_{32} \cdot \mathbf{x} - \omega_{32} t)}\} \right. \\
&\quad \left. + (\mathbf{e}_2 \times \mathbf{e}_3) \text{Im}\{E_2^* E_3 e^{i(\mathbf{k}_{32} \cdot \mathbf{x} - \omega_{32} t)}\} \right] \\
&\tag{C.7}
\end{aligned}$$

also from the definitions of the polarization vectors we can calculate the cross products

$$\begin{aligned}
\mathbf{e}_1 \times \mathbf{e}_2 &= \frac{(-k_{1x}, -k_{1y}, 0)}{\|\mathbf{k}_1\|^2} = -\hat{\mathbf{k}}_1 \\
\mathbf{e}_1 \times \mathbf{e}_3 &= \frac{(0, 0, -k_{1y}k_{3x} + k_{3y}k_{1x})}{\|\mathbf{k}_1\|^2 \|\mathbf{k}_3\|^2} = \mathbf{e}_z \sin \theta_{13} \\
\mathbf{e}_2 \times \mathbf{e}_3 &= \frac{(k_{3x}, k_{3y}, 0)}{\|\mathbf{k}_3\|^2} = \hat{\mathbf{k}}_3,
\end{aligned} \tag{C.8}$$

and putting everything together

$$\begin{aligned}
iu_v \mathbf{E}^* \times \mathbf{E} \cdot \hat{\mathbf{F}} &= -2u_v \left[-\hat{\mathbf{k}}_1 \text{Im}\{12\} + \mathbf{e}_z \sin \theta_{13} \text{Im}\{13\} + \hat{\mathbf{k}}_3 \text{Im}\{23\} \right] \cdot \hat{\mathbf{F}} \\
&= (\Omega_x, \Omega_y, \Omega_z) \cdot \hat{\mathbf{F}}
\end{aligned} \tag{C.9}$$

with

$$\begin{aligned}\Omega_x &= \frac{k_{1x}}{\|\mathbf{k}_1\|} \text{Im}\{\Omega_{12} e^{i(\mathbf{k}_{21} \cdot \mathbf{x} - \omega_{21} t)}\} + \frac{k_{3x}}{\|\mathbf{k}_3\|} \text{Im}\{\Omega_{23} e^{i(\mathbf{k}_{32} \cdot \mathbf{x} - \omega_{32} t)}\} \\ \Omega_y &= \frac{k_{1y}}{\|\mathbf{k}_1\|} \text{Im}\{\Omega_{12} e^{i(\mathbf{k}_{21} \cdot \mathbf{x} - \omega_{21} t)}\} + \frac{k_{3y}}{\|\mathbf{k}_3\|} \text{Im}\{\Omega_{23} e^{i(\mathbf{k}_{32} \cdot \mathbf{x} - \omega_{32} t)}\} \\ \Omega_z &= \text{Im}\{\Omega_{13} e^{i(\mathbf{k}_{31} \cdot \mathbf{x} - \omega_{31} t)}\},\end{aligned}\quad (\text{C.10})$$

and

$$\begin{aligned}\Omega_{12} &= 2u_v E_1^* E_2 \\ \Omega_{13} &= -2u_v E_1^* E_3 \sin \theta_{13} \\ \Omega_{23} &= -2u_v E_2^* E_3.\end{aligned}\quad (\text{C.11})$$

C.0.0.1 Going into rotating frame

This is where things start getting fun. We need to transform Eq. C.9 into the rotating frame. Which terms are ‘slow’ and we get to keep and which are ‘fast’ depends on the specific choice of Raman frequencies. Only the \hat{F}_x and \hat{F}_y operators are affected by the unitary transformation while \hat{F}_z remains unchanged. We therefore choose the beams that give a \hat{F}_z coupling to be close in frequency.

There are two different frequency choices which Dan calls ‘blue’ and ‘red’ detuned which are shown in Fig. 2, and they determine whether ω_{21} and ω_{31} are positive or negative. I’m not sure if we can generalize something at this point. Lets

look at the first term of the $\Omega_x \hat{F}_x$ coupling for practice.

$$\begin{aligned}
\Omega_x^{(1)} \hat{F}_x &\rightarrow \frac{1}{4i} \frac{k_{1x}}{\|\mathbf{k}_1\|} \left(\Omega_{12} e^{i(\mathbf{k}_{21} \cdot \mathbf{x} - \omega_{21})t} - \Omega_{12}^* e^{-i(\mathbf{k}_{21} \cdot \mathbf{x} - \omega_{21}t)} \right) \left(e^{i\omega_{RF}t} \hat{F}_+ + e^{-i\omega_{RF}t} \hat{F}_- \right) \\
&\approx \frac{1}{4i} \frac{k_{1x}}{\|\mathbf{k}_1\|} \left(\Omega_{12} e^{i(\mathbf{k}_{21} \cdot \mathbf{x} - (\omega_{21} \mp \omega_{RF})t)} \hat{F}_\pm - \Omega_{12}^* e^{-i(\mathbf{k}_{21} \cdot \mathbf{x} - (\omega_{21} \mp \omega_{RF})t)} \hat{F}_\mp \right) \\
&= \frac{1}{4i} \frac{k_{1x}}{\|\mathbf{k}_1\|} \left(\Omega_{12} e^{i(\mathbf{k}_{21} \cdot \mathbf{x} - (\omega_{21} \mp \omega_{RF})t)} - c.c. \right) \hat{F}_x \pm i \left(\Omega_{12} e^{i(\mathbf{k}_{21} \cdot \mathbf{x} - (\omega_{21} \mp \omega_{RF})t)} + c.c. \right) \hat{F}_y \\
&= \frac{1}{2} \frac{k_{1x}}{\|\mathbf{k}_1\|} |\Omega_{12}| \left(\sin[\mathbf{k}_{21} \cdot \mathbf{x} - (\omega_{21} \mp \omega_{RF})t + \phi_{12}] \hat{F}_x \pm \cos[\mathbf{k}_{21} \cdot \mathbf{x} - (\omega_{21} \mp \omega_{RF})t + \phi_{12}] \hat{F}_y \right)
\end{aligned} \tag{C.12}$$

Where the upper sign corresponds to the $\omega_{21} > 0$ case (blue detuned) and the lower sign to $\omega_{21} < 0$ (red detuned). Similarly, the second therm of $\Omega_x \hat{F}_x$ is

$$\begin{aligned}
\Omega_x^{(2)} \hat{F}_x &\rightarrow \frac{1}{4i} \frac{k_{3x}}{\|\mathbf{k}_3\|} \left(\Omega_{23} e^{i(\mathbf{k}_{32} \cdot \mathbf{x} - \omega_{32})t} - \Omega_{23}^* e^{-i(\mathbf{k}_{32} \cdot \mathbf{x} - \omega_{32}t)} \right) \left(e^{i\omega_{RF}t} \hat{F}_+ + e^{-i\omega_{RF}t} \hat{F}_- \right) \\
&\approx \frac{1}{2} \frac{k_{3x}}{\|\mathbf{k}_3\|} |\Omega_{23}| \left(\sin[\mathbf{k}_{32} \cdot \mathbf{x} - (\omega_{32} \mp \omega_{RF})t + \phi_{23}] \hat{F}_x \pm \cos[\mathbf{k}_{32} \cdot \mathbf{x} - (\omega_{32} \mp \omega_{RF})t + \phi_{23}] \hat{F}_y \right)
\end{aligned} \tag{C.13}$$

where I used the same sign convention as before. It is important to keep in mind though that if ω_{21} is positive then ω_{32} must be negative and vice versa. **Double**

check again that signs are correct! Let's continue with the algebra galore...

$$\begin{aligned}
\Omega_y^{(1)} \hat{F}_y &\rightarrow -\frac{1}{4} \frac{k_{1y}}{\|\mathbf{k}_1\|} \left(\Omega_{12} e^{i(\mathbf{k}_{21} \cdot \mathbf{x} - \omega_{21} t)} - \Omega_{12}^* e^{-i(\mathbf{k}_{21} \cdot \mathbf{x} - \omega_{21} t)} \right) \left(e^{i\omega_{RF} t} \hat{F}_+ - e^{-i\omega_{RF} t} \hat{F}_- \right) \\
&= \mp \frac{1}{4} \frac{k_{1y}}{\|\mathbf{k}_1\|} \left(\Omega_{12} e^{i(\mathbf{k}_{21} \cdot \mathbf{x} - (\omega_{21} \mp \omega_{RF}) t)} \hat{F}_\pm + \Omega_{12}^* e^{-i(\mathbf{k}_{21} \cdot \mathbf{x} - (\omega_{21} \mp \omega_{RF}) t)} \hat{F}_\mp \right) \\
&= \mp \frac{1}{4} \frac{k_{1y}}{\|\mathbf{k}_1\|} \left(\left(\Omega_{12} e^{i(\mathbf{k}_{21} \cdot \mathbf{x} - (\omega_{21} \mp \omega_{RF}) t)} + c.c. \right) \hat{F}_x + i \left(\Omega_{12} e^{i(\mathbf{k}_{21} \cdot \mathbf{x} - (\omega_{21} \mp \omega_{RF}) t)} - c.c. \right) \hat{F}_y \right) \\
&= \mp \frac{1}{2} \frac{k_{1y}}{\|\mathbf{k}_1\|} |\Omega_{12}| \left(\cos[\mathbf{k}_{21} \cdot \mathbf{x} - (\omega_{21} \mp \omega_{RF}) t + \phi_{12}] \hat{F}_x - \sin[\mathbf{k}_{21} \cdot \mathbf{x} - (\omega_{21} \mp \omega_{RF}) t + \phi_{12}] \hat{F}_y \right)
\end{aligned} \tag{C.14}$$

and

$$\begin{aligned}
\Omega_y^{(2)} \hat{F}_y &\rightarrow -\frac{1}{4} \frac{k_{3y}}{\|\mathbf{k}_3\|} \left(\Omega_{23} e^{i(\mathbf{k}_{32} \cdot \mathbf{x} - \omega_{32} t)} - \Omega_{23}^* e^{-i(\mathbf{k}_{32} \cdot \mathbf{x} - \omega_{32} t)} \right) \left(e^{i\omega_{RF} t} \hat{F}_+ - e^{-i\omega_{RF} t} \hat{F}_- \right) \\
&\approx \mp \frac{1}{2} \frac{k_{3y}}{\|\mathbf{k}_3\|} |\Omega_{23}| \left(\cos[\mathbf{k}_{32} \cdot \mathbf{x} - (\omega_{32} \mp \omega_{RF}) t + \phi_{23}] \hat{F}_x - \sin[\mathbf{k}_{32} \cdot \mathbf{x} - (\omega_{32} \mp \omega_{RF}) t + \phi_{23}] \hat{F}_y \right)
\end{aligned} \tag{C.15}$$

The complete Hamiltonian in the rotating frame after doing the rotating wave ap-

proximation is then

$$\begin{aligned}
\hat{H} = & \frac{1}{2} \frac{|\Omega_{12}|}{\|\mathbf{k}_1\|} \left(\left(k_{1x} \sin[\mathbf{k}_{21} \cdot \mathbf{x} - (\omega_{21} \mp \omega_{RF})t + \phi_{12}] \pm k_{1y} \cos[\mathbf{k}_{21} \cdot \mathbf{x} - (\omega_{21} \pm \omega_{RF})t + \phi_{12}] \right) \hat{F}_x \right. \\
& + \left. \left(\pm k_{1x} \cos[\mathbf{k}_{21} \cdot \mathbf{x} - (\omega_{21} \mp \omega_{RF})t + \phi_{12}] \mp k_{1y} \sin[\mathbf{k}_{21} \cdot \mathbf{x} - (\omega_{21} \pm \omega_{RF})t + \phi_{12}] \right) \hat{F}_y \right) \\
& \frac{1}{2} \frac{|\Omega_{23}|}{\|\mathbf{k}_3\|} \left(\left(k_{3x} \sin[\mathbf{k}_{32} \cdot \mathbf{x} - (\omega_{32} \mp \omega_{RF})t + \phi_{23}] \pm k_{3y} \cos[\mathbf{k}_{32} \cdot \mathbf{x} - (\omega_{32} \pm \omega_{RF})t + \phi_{23}] \right) \hat{F}_x \right. \\
& + \left. \left(\pm k_{3x} \cos[\mathbf{k}_{32} \cdot \mathbf{x} - (\omega_{32} \mp \omega_{RF})t + \phi_{23}] \mp k_{3y} \sin[\mathbf{k}_{32} \cdot \mathbf{x} - (\omega_{32} \pm \omega_{RF})t + \phi_{23}] \right) \hat{F}_y \right) \\
& + |\Omega_{13}| \sin(\mathbf{k}_{31} \cdot \mathbf{x} - \omega_{31}t + \phi_{13}) \hat{F}_z
\end{aligned} \tag{C.16}$$

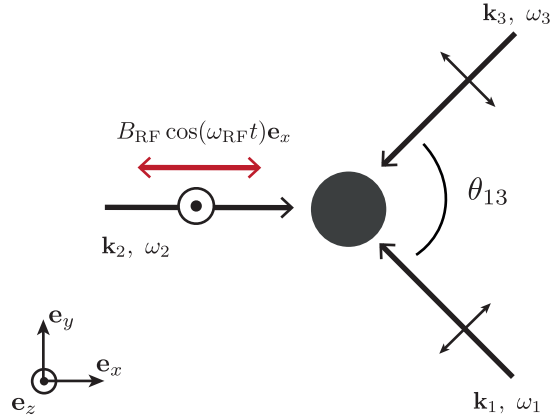


Figure 1: Laser layout: We use a strong RF field and three linearly polarized Raman beams propagating in the xy plane couple the $|xyz\rangle$ states and engineer the Rashba Hamiltonian.

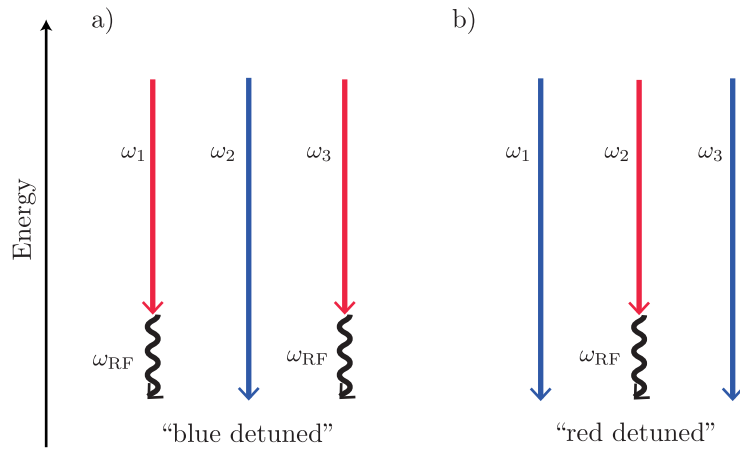


Figure 2: Laser frequencies: We have two frequency choices that allow us to address the three transitions between the $|xyz\rangle$ states. **a)** The blue detuned case. There are 2 frequencies smaller by about ω_{RF} and one larger frequency. **b)** The red detuned case. There are 2 frequencies that are larger by about ω_{RF} and one smaller frequency. Nice!

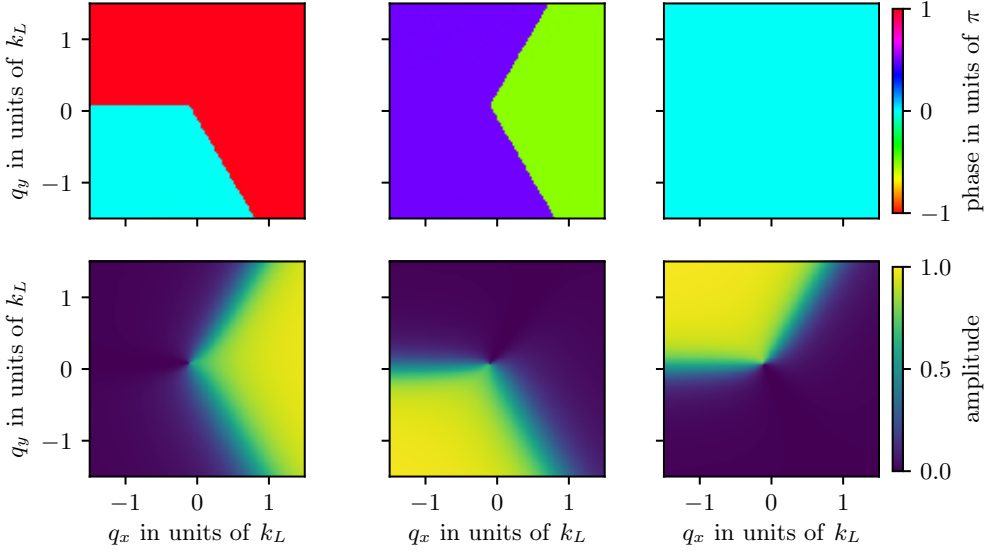


Figure 3: **a** Probabilities as a function of quasimomentum for the three output ports of the interferometer at $t_{\text{free}} = 160 \mu\text{s}$ **b** Probabilities as a function of free evolution time t_{free} for an input state with quasimomentum $(q_1, q_2) = (0.55, -0.92) k_L$ indicated by the blue star on **a** and in the topological ground branch ($n = 1$)

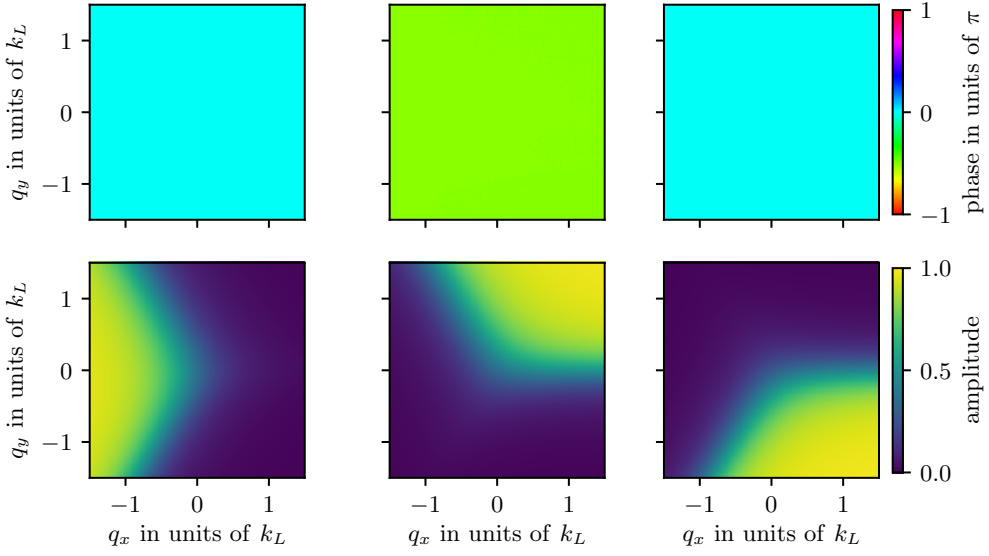


Figure 4: **a** Probabilities as a function of quasimomentum for the three output ports of the interferometer at $t_{\text{free}} = 160 \mu\text{s}$ **b** Probabilities as a function of free evolution time t_{free} for an input state with quasimomentum $(q_1, q_2) = (0.55, -0.92) k_L$ indicated by the blue star on **a** and in the topological ground branch ($n = 1$)

Bibliography

- [1] Roger Brown. *Nonequilibrium many body dynamics with ultracold atoms in optical lattices and selected problems in atomic physics*. PhD thesis, University of Maryland College Park, Digital Repository at the University of Maryland, 6 2014.
- [2] Creston D. Herold. *Ultracold mixtures of Rubidium and Ytterbium for open system quantum engineering*. PhD thesis, University of Maryland College Park, Digital Repository at the University of Maryland, 6 2014.
- [3] Abigail R. Perry. *An apparatus for light-less artificial gauge fields and new imaging techniques*. PhD thesis, University of Maryland College Park, Digital Repository at the University of Maryland, 6 2015.
- [4] B. P. Anderson and M. A. Kasevich. Loading a vapor-cell magneto-optic trap using light-induced atom desorption. *Physical Review A*, 63(2):023404, January 2001.
- [5] D. L. Campbell and I. B. Spielman. Rashba realization: Raman with RF. *New J. Phys.*, 18(3):033035, 2016.